Design and Anchorage Dependence of Shape Memory Alloy Actuators on Enhanced Voiding of a Bladder

Faezeh Arab Hassani, Gil Gerald Lasam Gammad, Roshini Priya Mogan, Tze Kiat Ng, Tricia Li Chuen Kuo, Lay Guat Ng, Percy Luu, Nitish V. Thakor, Shih-Cheng Yen, and Chengkuo Lee**

The use of shape memory alloy (SMA) actuators to restore voiding of bladder for myogenic under active bladder (UAB) patients is proposed recently. Even though previous work show the unique capability of this technology for bladder voiding, the low voiding volume and high energy consumption of the device limit the advancement of this technique. This study proposes a novel approach using an interlaced configuration to overcome these limitations. In this device, SMA actuators are threaded through rigid anchor points of the flexible vest. The novel anchorage of SMA actuators provides more conformability for the vest and lower energy consumption for the device, while the new interlaced configuration enhances the voiding volume. The device is tested initially on a rubber model for the bladder, then it is implanted in an anesthetized rat, and a voiding volume of more than 20% at 4 V is successfully achieved. A commercial force sensor is integrated with the device to make it suitable for neurogenic UAB patients. The sensor provides a feedback control signal to the patient to initiate the actuation of the device upon fullness of bladder. The overall system is a promising advance over the state-of-the-art providing bladder voiding in UAB patients.

1. Introduction

Shape memory property of some materials such as Nickel Titanium (NiTi) allows them to return to their original shape by applying heat; thus, these materials can be used as thermal actuators.[1] This shape transformation is caused by atomic-level structural changes in the material from the martensitic to the austenite phase at a specific temperature,[2] and applying voltage to the material is a method to induce heat for such transformation.[3] Voluntary repeatable shape transformation, material biocompatibility, and small weight of NiTi shape memory alloy (SMA) actuators make them suitable for medical applications.[4–12] Usage of NiTi SMA actuators for muscular contraction,[8] artificial anal sphincter,[7] urethral valve,[13] myocardium,[8] drug delivery system,[3] and most recently, voiding of a bladder,[14] has been reported.

The previous SMA-based actuator for voiding of a bladder consisted of a flexible vest that covered the bladder surface and physically contracted it upon the actuation of assembled SMA wires.[14] Since a fixed length was considered for SMA wires in this design, the device could be used for only one bladder size that was matched with the total inner diameter of actuator. The proposed design in our study has a more conformable vest that can be fitted for a wider range of bladder sizes in rats with similar body weight, and can substantially improve the voiding volume and energy consumption of the device.

The previous SMA-based actuator was proposed for assisting the detrusor muscle in myogenic underactive bladder (UAB) patient with detrusor muscle contractility disorder but intact nerves.[14] Our study broadens the application of the actuating device also to neurogenic UAB patients suffering from both damaged detrusor muscle and nervous system; these patients are not able to rely on the natural nerve pathways to realize

Dr. F. A. Hassani, Prof. N. V. Thakor, Prof. S.-C. Yen, Prof. C. Lee
Department of Electrical and Computer Engineering
Faculty of Engineering
National University of Singapore
4 Engineering Drive 3, E4 #05-45, Singapore 117583, Singapore
E-mail: shihcheng@nus.edu.sg; elelc@nus.edu.sg

Dr. F. A. Hassani, Dr. G. G. L. Gammad, R. P. Mogan,
Prof. N. V. Thakor, Prof. S.-C. Yen, Prof. C. Lee
Singapore Institute for Neurotechnology
National University of Singapore
28 Medical Drive #05-COR, Singapore 117456, Singapore

The ORCID identification number(s) for the author(s) of this article can be found under https://doi.org/10.1002/admt.201700184.

DOI: 10.1002/admt.201700184

Dr. F. A. Hassani, Prof. S.-C. Yen, Prof. C. Lee
Center for Intelligent Sensors and MEMS
National University of Singapore
5 Engineering Drive 1, E6 #05-11F, Singapore 117608, Singapore

Dr. T. K. Ng
Raffles Hospital
585 North Bridge Road, Singapore 188770, Singapore

Dr. T. L. C. Kuo, Dr. L. G. Ng
Singapore General Hospital
Outram Road, Singapore 169608, Singapore

Dr. P. Luu
Department of Surgery
Yong Loo Lin School of Medicine
National University of Singapore
IE Kent Ridge Road, Singapore 119228, Singapore

when their bladder is full. Hence, we propose to integrate a force sensor with the device to find out the bladder filling volume. When the bladder reaches its maximum volume, the force sensor will inform the patient to actuate the device. Several sensors, such as flexible strain, pressure, or tactile sensors,[15–26] can be integrated with the actuating device to sense the status of bladder fullness; however, to quantify the bladder fullness accurately, in our study we use a commercial force sensor to provide the feedback control signal to the patient.

We first present the design and fabrication of the interlaced actuating device followed by the numerical modeling of the forces exerted by the SMA wires on the vest. The proposed device was tested by using an antigravity experimental setup on a balloon. The antigravity experimental setup was suitable for recording the device operation during both the actuation and relaxation of SMA wires. The percentage of water voided, operational temperatures, and hysteresis behavior of the device are studied. The hysteresis behavior of the new interlaced device is compared with the recently proposed actuating device. We further demonstrate an in vivo test of the device in an animal model of bladder function. The percentage of saline voided from bladder after actuating the device is compared with the voiding volume of the previously proposed design. A commercial force sensor is integrated with the device, and its resistance change is used as a control feedback signal to predict the time that the bladder was full. The characterization of the force sensor is done by using a second experimental setup, which allows the gravitational voiding of water similar to the bladder voiding. Then, in vivo integration of the force sensor with the device is demonstrated in a rodent model of bladder function regulation. Finally, we discuss the importance of integration of a force sensor with the actuating device on shaping a feedback control system for patients with neurogenic bladder.

2. The Interlaced Actuating Device for Neurogenic UAB

Figure 1a shows how a healthy bladder is functioning during normal micturition. The stretch receptors in bladder wall send the bladder fullness signals via afferent fibers of the pelvic nerve toward the spinal cord and brainstem.[27–29] At the appropriate time for voiding, efferent fibers convey signals to initiate the detrusor muscles contraction and relaxation of sphincters.[27–29] As a result of UAB, the bladder is emptied partially and thus leads to overfilling and enlargement of bladder.[30] The causes for UAB are also summarized in Figure 1a. The device proposed in the previous work was used for voluntary voiding of the bladder upon sensation of fullness in myogenic UAB patients (Case 1).[14] By contrast, the proposed actuating device in this paper can be an alternative approach to the treatment for neurogenic UAB patients (Case 2). Figure 1b shows the schematic contraction of the actuating device integrated with a force sensor, and the consequent activation of the device and voiding of the bladder after receiving a signal from the force sensor. A force sensor was integrated inside the vest. During filling of the bladder, the bladder gradually exerted a force onto the sensor that decreased the resistance. After observing the maximum resistance drop, as a sign of a full bladder, the device was actuated by applying a voltage to the SMA wires. The actuation of the device also caused a drop in the resistance of sensor that may be used as an indicator for the contraction of the SMA wires.

2.1. Actuating Device Design and Fabrication

The previously proposed actuating devices consisted of three NiTi SMA wires with the maximum length of 9 mm and diameter of 200 μm that were purchased from Dynalloy Inc. (Irvine, CA). The SMA wires were crimped on both ends with brass crimps and glued in parallel configuration onto the fingers of vest, referred here as the parallel device. The vest consisted of three rings that were connected at two joints (Figure S1a, Supporting Information). The design of the vest was optimized for achieving the highest deformation under the forces imposed by SMA wires. The SMA wires showed a resistivity of 29 Ω m^{-1}.[31] However, after the crimping and soldering, the resistance increased to about 0.7 Ω. Each wire was contracted up to 4.5%, $\Delta L/L$ (L is the length of the wire while ΔL is the change in the length) after voltage application thus exerting a force onto the vest. The schematic view of the parallel device is shown in Figure S1a (Supporting Information). In contrast to this design, the actuating device in our study is composed of two 5.5 cm length NiTi SMA wires that are covered with a 4.5 cm length silicone tubing and threaded through the anchor points on a flexible vest in an interlaced configuration. **Figure 2**a shows the schematic of the assembled vest with SMA wires wrapped with silicone tubing. The back view of the vest is also shown in Figure 2a. The vest had an inner diameter of 1 cm to match the normal size of a rat's bladder, and thickness of 1 mm to allow the vest to conform well to the bladder and three separate rings connected at two joints to be able to observe the bladder surface during the actuation of device. Each 0.5 cm end of the SMA wires was covered with a copper tape to ease the connection of power source to the device. 2.5 cm of each SMA wire was used to keep the distance between two facing anchor points of each ring at 9 mm. Since the voltage was applied to the both SMA wires simultaneously, the remaining 2 cm of each SMA wire was considered to not contribute to the deformation of the device while connecting it to the power source. The diameter of the SMA wires and the design of the vest for the interlaced device were the same as the parallel device.

Fixing of SMA wires is usually done by crimping/crushing the wire inside a tube or fixing it to a solid part with the help of screws and bolts. Since the vest in our design is flexible, we designed a solid anchor point with a hole with diameter of 1.5 mm to allow the silicone tube and SMA wire pass through it with enough room for the tube to move freely while the bladder was filling or emptying. The anchor point (Figure 2a) was designed in SOLIDWORKS and 3D printed by using a transparent solid material (i.e., VeroClear-RGD810).[32] The anchor points were then glued on the end of each finger. Since the crimping of SMA wires was no longer needed and was replaced with anchor points, the previous increase of resistance in the parallel design due to crimping was resolved. Both ends of each

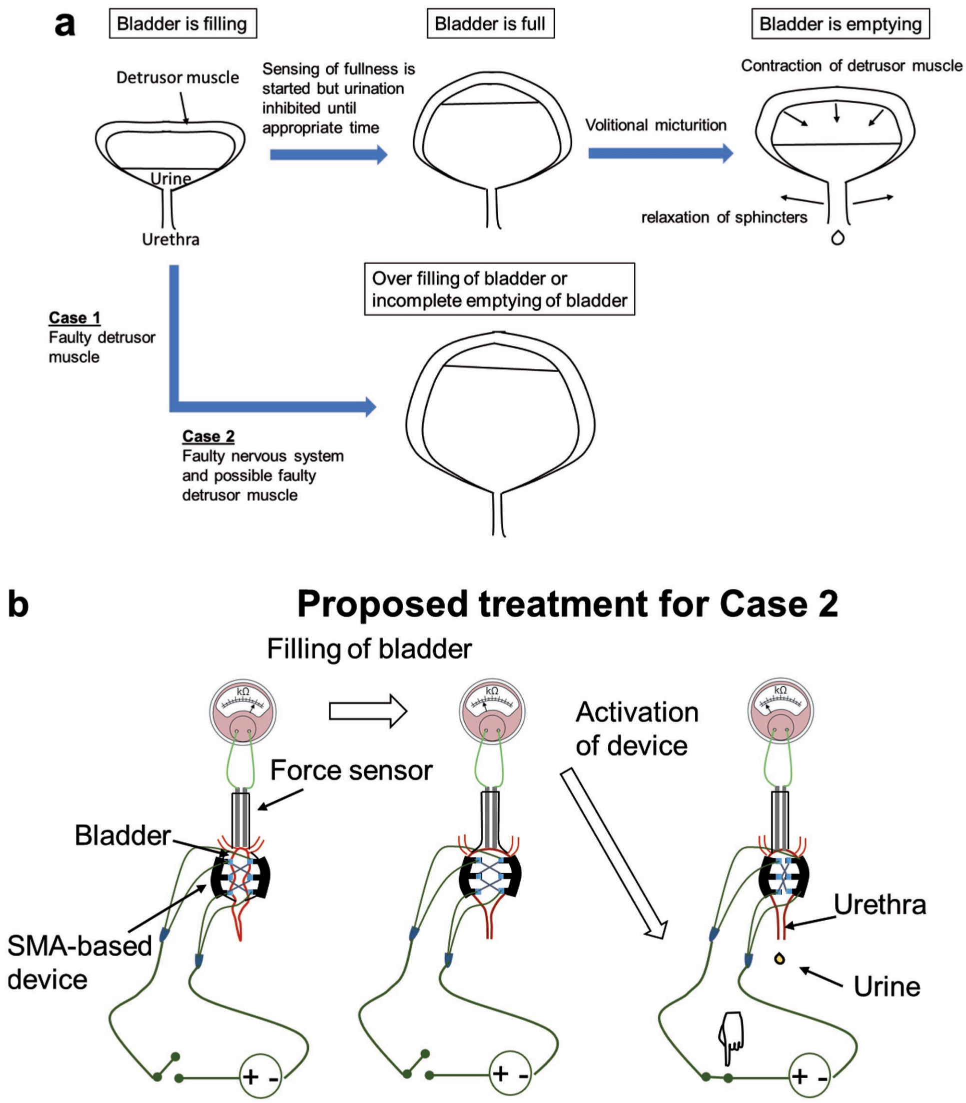

Figure 1. The process of micturition in a healthy bladder versus UAB cases. a) The volitional micturition and UAB cases. b) The operation of the proposed treatment for case 2.

silicone tubing were sealed by using stainless steel staples in order to keep the effective wires length, controlled by the vest, to 2.5 cm, and avoid future possible contact of body fluid with SMA wires.

The flexible spherical vest in Figure 2a was designed in SOLIDWORKS and 3D printed by using a flexible rubber-like material (i.e., TangoBlackPlus) with a Young's Modulus, E, of 0.3 MPa,[32] and a density of 1130 kg m^{-3}.[33] The low thermal conductivity of silicone polymer (i.e., 0.2 W m^{-1} K^{-1})[34,35] made it a suitable thermal insulation layer for the SMA wires to reduce the heat transfer to the balloon, and later to the bladder. Therefore, medical grade silicone tubing (Silcon) with inner diameters of 500 µm and outer diameters of 965 µm was used as the thermal insulation layer for the SMA wire. Figure 2b presents the fabricated device that was put on a balloon model of the bladder filled with water. After applying voltage to the device, the SMA wires were heated to the transition temperature of 70 °C and contracted up to 4.5%, and consequently applied a force to the vest. Due to the interlaced configuration for SMA wires, the middle anchor points were experiencing more force than that of the SMA wires in the parallel device. The deformation of the vest compressed the balloon or bladder, which then led to voiding. The vest performance was numerically modeled in COMSOL in order to find out the pressure distribution in the vest due to the forces exerted from SMA wires. The SMA wires were excluded from the numerical modeling. Instead, displacement loads were applied to the tip of each finger to model the effect of forces. The displacement loads were calculated based on the maximum 4.5% contraction of the SMA wires. The threading configuration and related dimensions are shown in Figure 2c. The displacement loads, in y-axis and z-axis directions, applied to each finger are calculated as following

$$\overrightarrow{u_n} = \left(\overrightarrow{u_{ny}}, \overrightarrow{u_{nz}}\right) = \left(\pm\|\overrightarrow{u_n}\|\cos\alpha, \pm\|\overrightarrow{u_n}\|\sin\alpha\right) \tag{1}$$

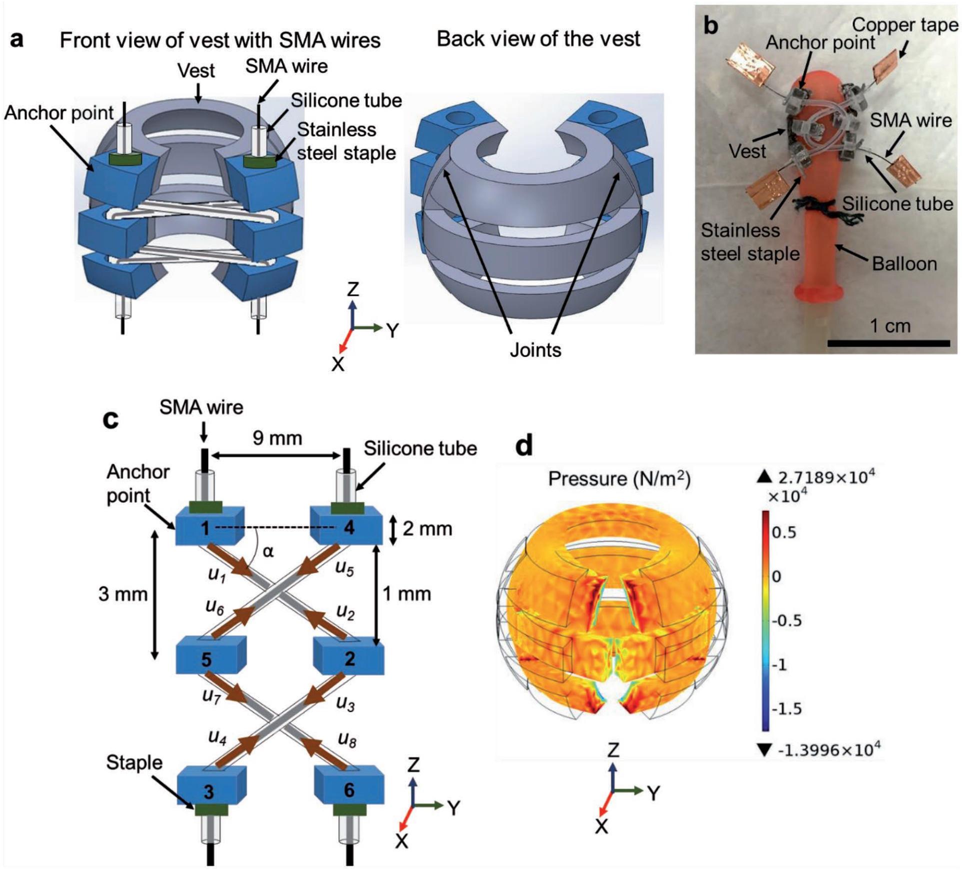

Figure 2. The design, modeling, and fabrication of the interlaced actuating device. a) The schematic front and back views of the vest as well as the threaded SMA wires in an interlaced configuration. b) The fabricated device on a balloon filled with water. c) The schematic illustration for the displacement loads applied to the tip of fingers for the modeling. d) The pressure distribution in the vest under displacement loads.

$$\|\overrightarrow{u_n}\| = \frac{4.5\%}{2} \times l \tag{2}$$

where $\overrightarrow{u_n}$ is the displacement load vector for each anchor point, $\|\overrightarrow{u_n}\|$ is the magnitude of the vector, $n = 1{:}1{:}7$ is the number of displacement load vectors, $l = 9.48$ (as shown in Figure 2c), and $\alpha = 18.45°$ is the angle between the SMA wire and y-axis. The total load applied onto each anchor point is calculated as following

$$\begin{aligned}
&\text{Anchor point 1}: \overrightarrow{u_1} = (-0.0657\ \text{mm}, -0.2025\ \text{mm}) \\
&\text{Anchor point 2}: \overrightarrow{u_2} + \overrightarrow{u_3} = (0\ \text{mm}, -0.405\ \text{mm}) \\
&\text{Anchor point 3}: \overrightarrow{u_4} = (0.0657\ \text{mm}, -0.2025\ \text{mm}) \\
&\text{Anchor point 4}: \overrightarrow{u_5} = (-0.0657\ \text{mm}, -0.2025\ \text{mm}) \\
&\text{Anchor point 5}: \overrightarrow{u_6} + \overrightarrow{u_7} = (0\ \text{mm}, -0.405\ \text{mm}) \\
&\text{Anchor point 6}: \overrightarrow{u_8} = (-0.0657\ \text{mm}, -0.2025\ \text{mm})
\end{aligned} \tag{3}$$

Figure 2d shows the pressure distribution of the vest under applied loads in Equation (3). The black solid lines in Figure 2d show the device before deformation. Figure S1b,c (Supporting Information) shows forces applied to the vest and the resulting pressure distribution for the parallel device. The displacement load vectors for the parallel device are calculated in Equations S1–S3 in the Supporting Information. The proposed interlaced configuration in this study increased the maximum pressure in vest (Figure 2d) for more than four times compared to the parallel device (Figure S2c, Supporting Information).

2.2. The Bench Top Study by Using an Antigravity Experimental Setup

Figure 3a shows the experimental setup to measure the amount of water voided from a balloon with a size similar to the bladder of a rat. As shown in Figure 3a, the device was placed on an empty balloon, which was then filled with water using a syringe. A power source was used to apply voltage to the device, and the displaced volume of water, ΔV, was read by a syringe that had its plunger removed. Figure 3b shows changes in the water level in the syringe upon voltage application to the device. The tube connected to the balloon had an internal diameter of 2.6 mm, while the internal diameter of the tube exiting from the 3-way stopcock was 0.5 mm. The maximum volume of water, V, the balloon could hold without overflowing the excess amount through the reading gauge, was 1 mL for the device, similar to the bladder of the rat.

In order to learn about the effects of voltage on the percentage of voiding volume, $\Delta V/V$, we applied voltages of 3,

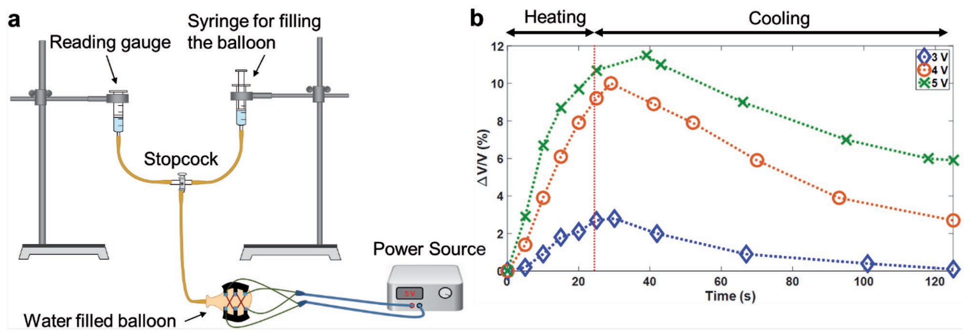

Figure 3. The benchtop experiments for the interlaced actuating device on a rubber balloon. a) The antigravitational balloon measurement setup. b) $\Delta V/V$ versus time curve for the applied voltages of 3, 4, and 5 V.

4, and 5 V to the device, and the $\Delta V/V$ as a function of time is shown in Figure 3b. A $\Delta V/V$ of 2.8% was obtained after applying 3 V for 25 s. Figure 3b shows that, by increasing the voltage to 4 and 5 V, a larger $\Delta V/V$ values of 10 and 11.5% were achieved, respectively. After removing the voltage, the SMA wires tended to recover to their original lengths. It took about 5 s for the SMA wires after removing the voltage of 3 and 4 V to start the cooling process and the wires continued to contract during this 5 s. This time was increased to about 9 s for 5 V voltage application. The benefit of using an antigravity setup (Figure 3a) for the characterization of the device was that we could also observe the behavior of wires during the cooling process. It is important to note that, even though a higher voiding could be achieved by increasing the stimulation duration or increasing the voltage, the higher induced temperatures in the wires may damage the balloon. Moreover, overheating the SMA wires with a larger voltage level or for a longer period of time could result in the weakening of the memory effect and thus reducing the lifetime of the wires. For this reason and also in order to keep the temperature change in the SMA wires nearer to the animal's body temperature,[36] we used the optimum voltage of 4 V for the implantation of the device in a rat model.

The maximum temperature of the SMA wire versus $\Delta V/V$ is presented in **Figure 4**a for 4 V applied voltage by using a FLIR E5 thermal imaging camera (Wilsonville, OR). The temperatures on the silicone tube and on the surface of the balloon were also checked by using a two channel HH506RA thermometer (Stamford, CONN). One K-type thermocouple was positioned on the surface of the silicone tube, and the other one was placed underneath the tube on the balloon surface. Kapton tape was used to fix the thermocouples in place, which might have caused the measured temperatures to be a bit higher than the real temperature values. Figure 4a plots the maximum temperature versus time for the SMA wire, the silicone tube, and the balloon surface. The optical and thermal images of the device under 4 V stimulation after 25 s are shown in Figure 4b. Figure 4c shows the positions of the thermocouples, and the temperatures of both channels at 25 s. The temperature reduction of about ≈13 °C between the surface of the SMA wire and the silicone tube was due to the thermal insulation of the silicone tube. A further 12 °C reduction in temperature was seen on the balloon surface due to the thermal conduction through the balloon surface and the air gap between the silicone tube and balloon surface.

The contraction of the device exhibits hysteresis, similar to the temperature-strain changes in the SMA wires.[31,37] The hysteresis behavior of the interlaced device is compared with that of the parallel device in Figure 4d. The interlaced device reached the maximum temperature of 69.6 °C after 25 s of voltage application (heating of wires), after which temperature started to decrease (cooling of wires). The maximum $\Delta V/V$ of 10% achieved 5 s after removing the voltage at the temperature of 60 °C while the maximum 5.9% voiding for the parallel device reached at the highest temperature of 83.4 °C. As shown in Figure 4d, the interlaced device is able to reduce the maximum temperature for 13.8 °C.

2.3. In Vivo Animal Test of the Actuating Device

The actuating device was implanted onto the bladder of an anesthetized rat, as shown in **Figure 5**a. In this setup, we used a precision balance to weigh the volume of the liquid voided from the bladder after the actuation of the device. The details of the surgical procedures are explained in the Experimental Section. As shown in Figure 5a, normal saline was used to fill the bladder up to 0.28 mL via a catheter inserted in the ureter. We stopped the saline infusion as soon as the liquid started to void from urethra. A voltage of 4 V was applied to the SMA wire device for 25 s, and the urine voided during this time was collected and weighed. Considering a measured density of 1.0012 kg L^{-1} for urine (the method for measuring the density is described in the Experimental Section), a $\Delta V/V$ of 23.59% was achieved for the device. The exact amount of the liquid volume voided from bladder was refilled to the bladder again, and the actuation process is repeated for the second time. A $\Delta V/V$ of 16.24% was achieved for the second time. The bladder voiding under 4 V application for 25 s for the first and second actuations is presented in Movies S1 and S2 (Supporting Information), respectively. Figure 5b–e shows the implanted device before and during 25 s actuation of the device for the first actuation. The voiding was completed 13 s after starting to apply the voltage to the device for the first time of actuation, while this time was measured for 9 s for the second time actuation. Even the SMA wires continued to contract after 13 s in the first actuation, but no more voiding was observed. This may be explained due to the fact that the continuing contraction forces were not enough to overcome the urethral resistance.

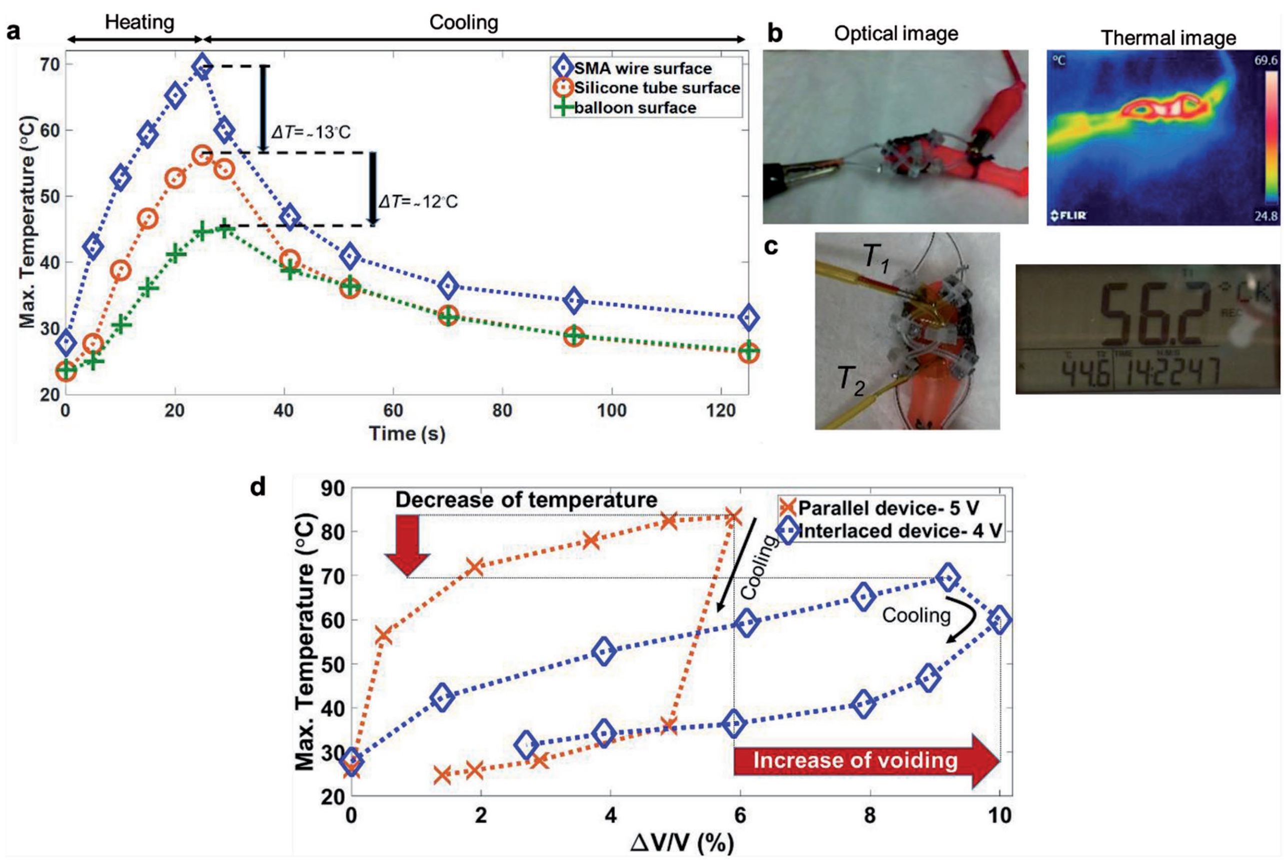

Figure 4. The temperature of the interlaced actuating device during operation. a) Maximum temperature versus time characteristics for the SMA wire surface (taken by the thermal camera), silicone tube surface, and the balloon surface (measured by the two channels thermometer). b) The optical and thermal images of the device at 25 s for the applied voltage of 4 V. c) The connected thermocouples on the SMA wire and balloon surface and the measured temperatures of channels (T_1 and T_2) at 25 s for the applied voltage of 4 V. d) The comparison of maximum temperature versus $\Delta V/V$ plot for the previously proposed parallel device and the new interlaced device in this study.

This shows that we could limit the time duration for applying voltage to 13 s. This shorter duration time for the voltage application will also help to avoid the overheating of the SMA wires. Figure 5f presents the average value of $\Delta V/V$ measured for the rat for both interlaced and parallel devices. The interlaced device increased the maximum voiding volume to 23.59% from the maximum voiding volume of 8.12% for the parallel device. The voiding percentage of 23.59% was larger than the experimental voiding result in Figure 3b, which showed a $\Delta V/V$ of 10%. One reason for the difference was the fact that the water displacement from the balloon in the setup shown in Figure 3a was pushing against gravity into the reading gauge. For this reason, we also measured the voiding volume by disconnecting the outlet tube from the reading gauge in Figure 3a, and let the water to be voided into a petri dish. This increased the voiding percentage to 16.51%. The balloon voiding in petri dish under 4 V application for 25 s is shown in Movie S3 (Supporting Information). Young's Modulus of the bladder muscle is at least two orders of magnitude smaller than that of the rubber balloon,[38] therefore a higher value of $\Delta V/V$ was not unexpected.

The optical image and thermal images of the implanted device in the rat over time are shown in Figure 5g. The temperature of a point on the bladder surface (Sp1) is shown with a cross in each of the images. The first optical image shows the device on the bladder. The temperature of Sp1 was raised from 31.9 °C at $T = 0$ s (voltage ON) to 33.7 °C at $T = 20$ s (voltage OFF). Since the voiding started and completed after about 13 s of applying 4 V to the device (Movie S1, Supporting Information), it would not be necessary to continue the voltage application beyond 13 s as no more voiding was observed. The temperature on the surface of silicone tube (Figure 4a) was measured about 33.86 °C while the temperature on the surface of bladder (Figure 5g) was about 33.3 °C, and which is below the normal temperature of animal's body.[39]

With 4 V stimulation, the current through wires was measured of 1.6 A. A rat voids the bladder completely one time per 327 s.[40] Figure 5h illustrates the percentage of the urine in the bladder, V_b/V, during 327 s for a healthy rat bladder, interlaced and parallel devices upon actuation. Figure 5h also presents the total energy consumption of interlaced and parallel devices during 327 s. By assuming that, a rat voided the bladder over 5 s and by considering a constant filling rate for the bladder during 322 s, the interlaced device should be actuated 4 times. Considering the voiding volume of 23.59% for the device in each actuation cycle, an energy consumption of 23.04 mA h was calculated for the interlaced device during 327 s. However, this value was increased to 54.56 mA h for the parallel device which required 10 times of actuation within the same time duration due to the

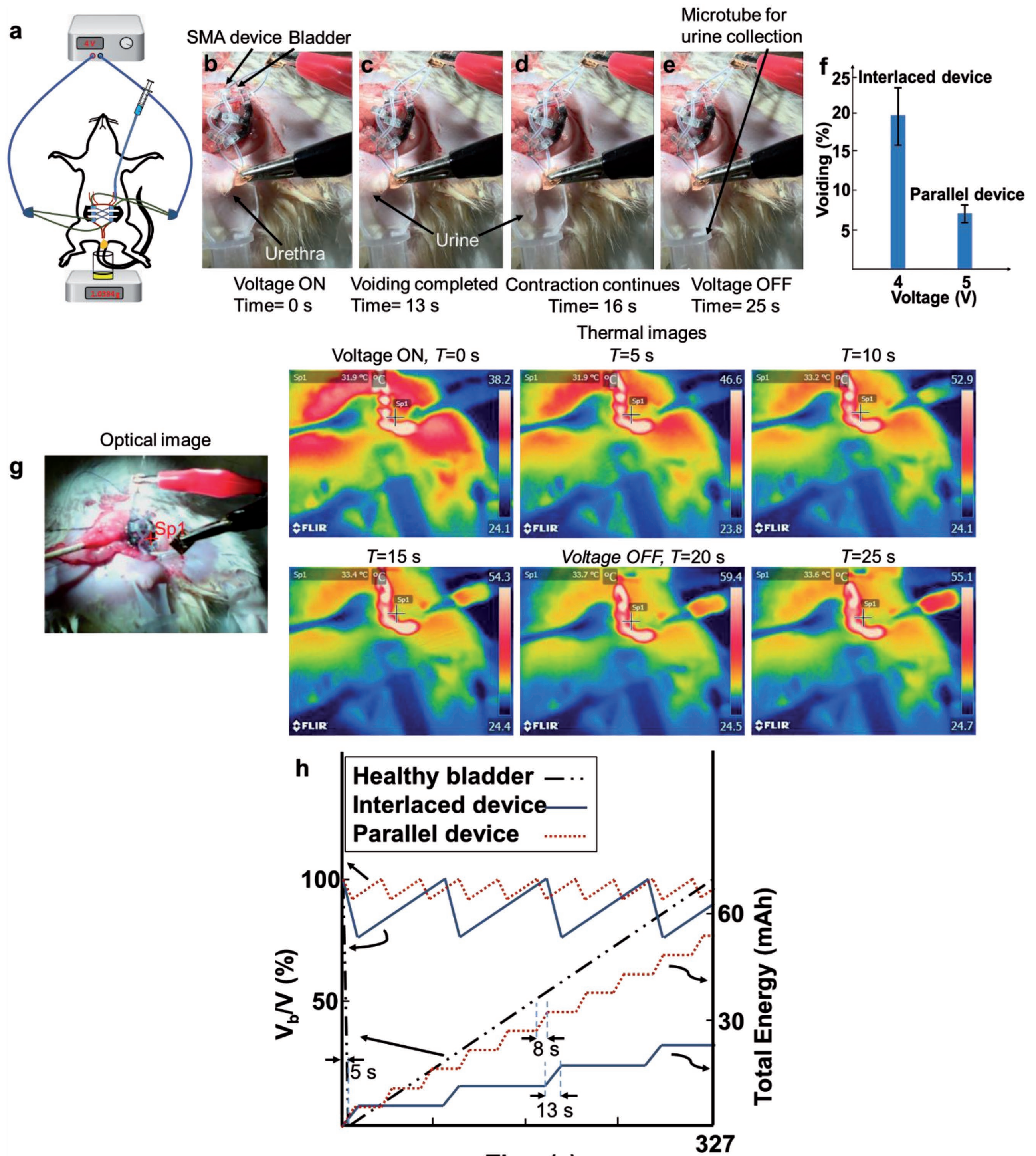

Figure 5. The in vivo test of the interlaced actuating device in a rat. a) The animal test setup. b–e) The voiding process during 25 s of 4 V voltage application. f) The mean average for the percentage of voiding for the interlaced and parallel devices for two times of actuations. g) Optical and thermal images of a spot on the bladder surface (Sp1) at various times of experiment. h) The percentage of urine volume in the bladder (V_b/V) versus time curves for a healthy rat bladder (one time of voiding), interlaced device (4 times of voidings), and parallel device (10 times of voidings); comparison of the total energy consumption versus time plots for interlaced and parallel devices after multiple actuations during 327 s.

lower voiding volume of 8.12%. As a result, the proposed interlaced device could not only enhance the voiding volume, but also reduced the energy consumption of the device. This energy saving property of the device makes it more suitable for its future integration with flexible energy harvesters,[41,42] raising the potential for a self-sustainable biomedical device. Table S1

(Supporting Information) compares the voiding percentage, power consumption per each cycle of actuation, and number of actuation cycles required per 327 s.

The size of rat's bladder can be varied from animal to animal even if they have the same body weight. The parallel device with the vest diameter of 1 cm was only fitted to the bladder sizes with the volume size of about 1 mL due to the fixed 9 mm length of SMA wires. The parallel actuation device was not able to compress smaller size of bladders in which the surface of bladder was not in contact with the vest. On the other hand, the SMA wires in the interlaced actuation device could move freely through anchor points, thus the device with the vest diameter of 1 cm could be fitted to a bladder size with the volume of 0.28 mL up to the volume size of about 1 mL.

2.4. Integration of the Actuating Device with a Force Sensor

Since neurogenic UAB patients may suffer from loss of sensory feedback signals during the filling of the bladder, it is necessary to integrate a sensor with the actuating device that can continuously inform the patient by sending a feedback signal on the filling status of the bladder. Therefore, the patient will figure out the right time to initiate the device actuation and voiding. Any sensor (e.g., force, pressure, strain) that can convert the information of the bladder volume status to an electrical signal is suitable to replace the missing sensory signals in the body. The current commercial pressure catheters are able to measure the pressure inside the bladder directly.[43] However, the catheter should be inserted through urethra, or via a surgery through an incision in the bladder wall that is cumbersome and invasive. For this reason, using of flexible sensors,[15–26] that could be fixed on the surface of bladder or inside the vest, may provide the information on the bladder filling status without the need of making an incision in the bladder wall.[44,45] In our study, we used a commercial FlexiForce force sensor (South Boston, MA) to accurately quantify the effect of bladder filling on the resistance change of the sensor. More information on the sensor is provided in the Experimental Section. The sensor showed a large resistance when no force was applied onto the sensor, while the resistance reduced after applying force to the sensing area of the sensor. The calibration of the sensor was conducted by using several precision weights. The plots of sensor resistance, R, versus force, as well as, sensor conductance, G, versus force and its linear fit curve are shown in Figure S2 (Supporting Information). The force sensor has a force sensing range up to 4 N.

2.4.1. The Bench Top Test of the Integrated Force Sensor by Using a Gravitational Setup

Since the width of the sensor was 14 mm and larger than the diameter of the vest, we bended the sensor by using a strap along AA′ line in the schematic view in **Figure 6**a to fit the sensor inside the vest. Even, the substrate of the sensor was polyester,[46] and was to some extent bendable at the sensing area, it caused the deformation of the vest. Also, it occupied a part of the volume inside the vest, therefore, V is reduced to 0.9 mL. Moreover, a larger voltage of 5 V was needed for voiding to compensate the stiffness of the force sensor that limited the deformation of the vest. The integrated force sensor with the actuation device is shown in Figure 6b, and then a balloon was placed inside the vest to cover the sensing area, and filled with water (Figure 6c). The schematic cross section of the device in Figure 6c along the dotted line is shown in Figure 6d. The forces exerted onto the sensor from the balloon, F_b, or the vest upon the actuation of SMA wires, F_d, as shown in Figure 6d. Therefore, a change in resistance was observed while filling the balloon with water, and also actuating the device. Smaller force sensors with a width of 7 mm showed no change in resistance by filling the balloon. We used a new gravitational voiding setup (**Figure 7**a) for the characterization of the force sensor integrated with the actuating device that is more similar to the urinary system. In this setup, a syringe pump was used to infuse water to the balloon and monitor changes in the

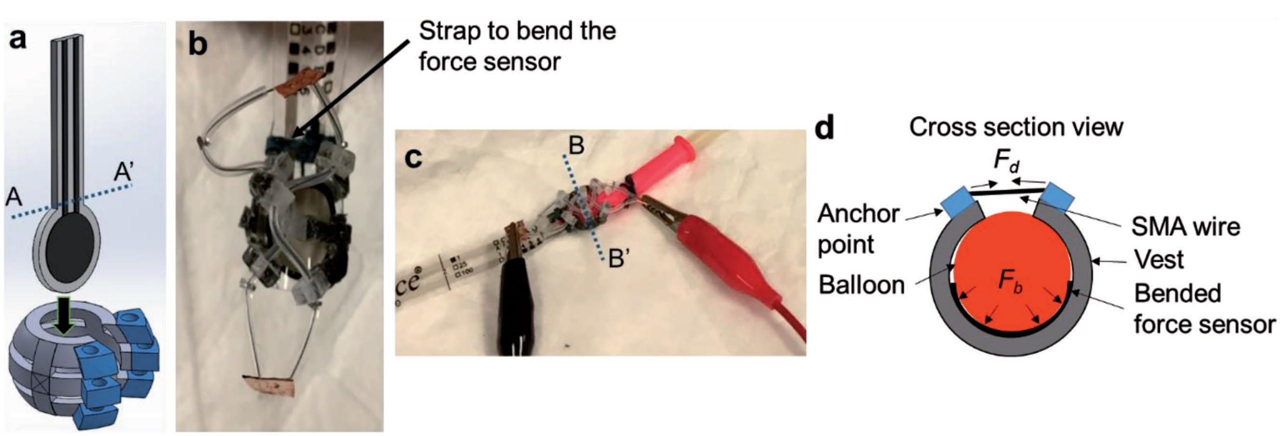

Figure 6. Integration of the force sensor with the interlaced actuating device. a) The schematic view for the integration of the bended force sensor (along the dotted AA′ line) with the vest. b) The integrated force sensor with the actuating device (a strap was used to bend the sensor). c) The application of the device and integrated force sensor on the balloon. d) The cross section of the device along the dotted BB′ line in (c) and the exerted forces from the balloon and device onto the force sensor.

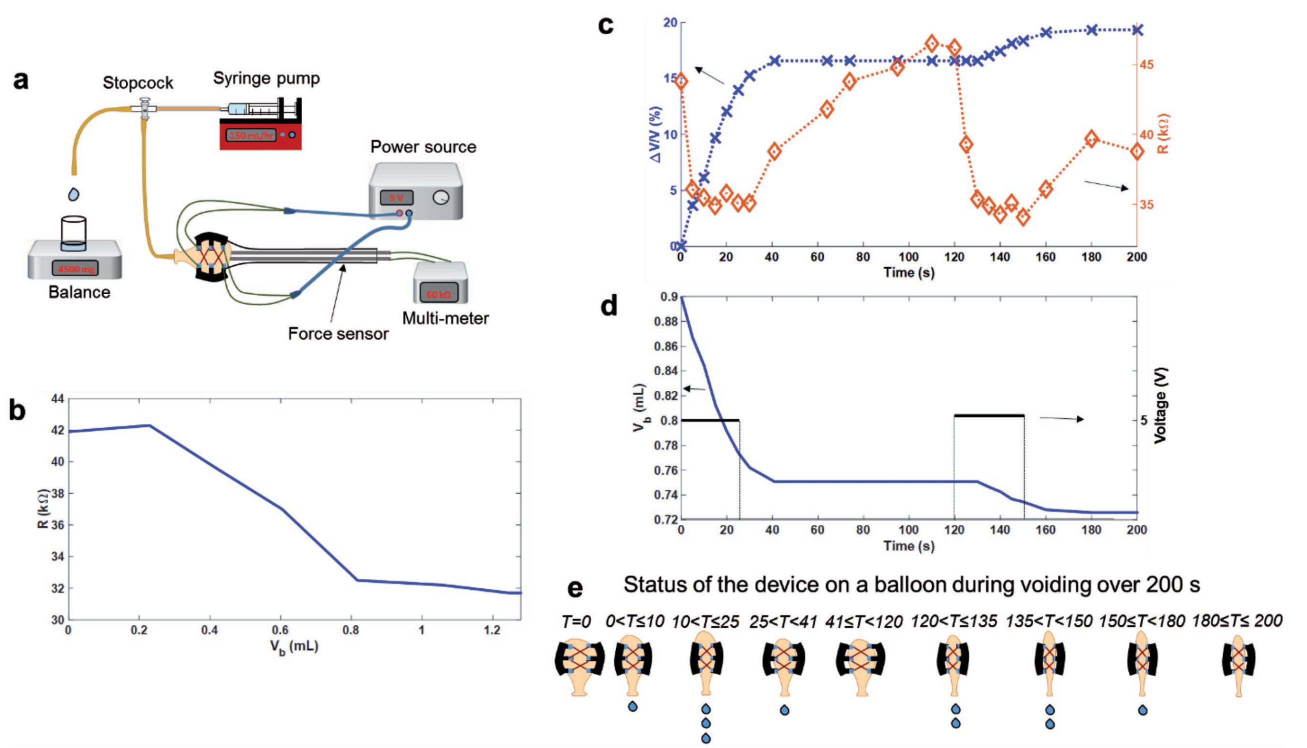

Figure 7. The benchtop experiments for the interlaced actuating device integrated with the force sensor on a rubber balloon. a) The gravitational balloon measurement setup. b) The plot of changes in the water volume, V_b, versus resistance. c) The plot of percentage of voided water and R versus time. d) The plot of voltage and V_b versus time. e) Schematic illustrations for the device at various times during the experiment.

resistance of the sensor. After the actuation of the device, the water voided from the balloon was continuously measured by using a precision balance.

Figure 7b presents the plot of R versus water volume in the balloon, V_b, which was derived by using the gravitational voiding setup in Figure 7a. The syringe pump was set to infuse the water with a constant rate of 2.5 mL min^{-1}. By increasing V_b from 0 to 0.9 mL, R was reduced from 41.9 to 32.25 kΩ. Referring to G versus force curve in Figure S2 (Supporting Information), F_b = 0.22 lbs (= 0.98 N) was exerted from the balloon onto the sensor. After that we activated the device two times to study the effect of forces applied to the sensor by the contraction of SMA wires. Figure 7c shows the plot of $\Delta V/V$ and R versus time. Figure 7d presents the voltage and V_b plots over the same time duration of Figure 7c. The schematic views of the status of the device in various times of the experiment are shown in Figure 7e: (i) $T = 0$ s, the balloon had the maximum volume of 0.9 mL; the voltage was turned ON thus a sudden force was applied to the vest and sensor, (ii) $0 < T \leq 10$ s, $\Delta V/V$ was increased to 5.55%; R was reduced from 43.8 kΩ at $T = 0$ s to 35.5 kΩ due to the contraction of SMA wires, the equivalent F_b was about 0.16 lbs (= 0.71 N), (iii) $10 < T < 25$ s, $\Delta V/V$ continued to increase; R was slightly reduced since SMA wires gradually continued to contract due to the voltage, (iv) $T = 25$ s, $\Delta V/V$ was reached 12.59%; voltage was turned OFF, (v) $25 < T \leq 41$ s, $\Delta V/V$ increased to 14.93%; R was constant for about 5 s after the removal of voltage similar to Figure 3b, and then started to increase since SMA wires started to recover to their original lengths, (vi) $41 \leq T < 120$ s, $\Delta V/V$ was constant at 14.93%; R reached to 46.2 kΩ that was larger than R = 43.8 kΩ at $T = 0$ s. This was due to the fact that balloon was voided about 15% compared to $T = 0$ s thus less force was exerted from the balloon onto the sensor, (vii) $T = 120$ s, V_b = 0.7507 mL; the voltage was turned ON thus a sudden force was applied to the vest and sensor, (viii) $120 < T \leq 135$ s, $\Delta V/V$ increased to 15.35%; due to the contraction of the SMA wires, R reduced from 46.2 to 35.4 kΩ, the equivalent F_b was about 0.22 lbs (= 0.97 N), (ix) $135 < T < 150$ s, $\Delta V/V$ increased to 16.55%; the SMA wires continued to contract and R was slightly reducing, (x) $T = 150$ s, $\Delta V/V$ = 16.55%; voltage was turned OFF thus R was almost constant for 3 s and started increase afterward, (xi) $150 < T \leq 180$ s, because of the better conformability of the device in this study, the voiding continued for the second actuation of the device up and it reached to $\Delta V/V$ = 17.41% at $T = 180$ s; (xii) $180 < T \leq 200$ s, $\Delta V/V$ stayed constant; since the balloon was voided compared to $T = 0$ s, the vest did not recover to its un-deformed shape similar to the vest at $T = 120$ s. As a result the force from the vest onto the sensor was not removed completely and R did not increase further.

The bending of force sensor caused a reduction of the starting resistance (Figure 7c) compared to that of the flat sensor (Figure S2, Supporting Information). Figure S4 (Supporting Information) shows the plot of $\Delta V/V$ and R versus 15 s of 5 V voltage application that was repeated for three times of the actuation. The changes in the starting resistance of the force sensor for three actuations were negligible, therefore, the possible effect of bending on the sensitivity of sensor can be ignored.

2.4.2. The In Vivo Animal Test of the Integrated Force Sensor

The setup in Figure 7a was used to characterize the force sensor integrated with the vest in an anesthetized rat. Changes in R were monitored during filling of the bladder with normal saline. The filling rate for the syringe pump was set to 200 µL min^{-1} and the infusion was continued until the liquid started to void through the urethra. $V = 1$ mL was measured for this rat. Important to note that the bladder size of the rat was larger than that of the previous rat used for the in vivo test of the actuating device. **Figure 8**a demonstrates the plot of R versus the volume of water in the bladder, V_b. Similar to Figure 7b, R started to decrease by increasing V_b. R decreased slightly from 64.2 kΩ at $T = 0$ s to 62.9 kΩ at $T = 240$ s. However, the decrease was more rapid from $R = 62.9$ kΩ at $T = 240$ s to $R = 57$ kΩ at $T = 300$ s. The equivalent force exerted from the bladder to the sensor, F_b, was about 0.05 lbs (= 0.22 N). The device was actuated by applying 5 V to the device and the plot of R versus time is shown in Figure 8b. At $T = 0$ s the bladder was full, and by turning the voltage ON, the sudden contraction of the SMA wires resulted in the reduction of R value from 52.6 to 45.6 kΩ at $T = 10$ s. R became almost constant till $T = 25$ s. After removing voltage at $T = 25$ s, R was constant for 5 s similar to Figure 7c. Then, SMA wires started to recover to their initial lengths. Therefore, the force exerted on the sensor reduced and led to an increase in R. R reached the maximum value of 60.6 kΩ at $T = 40$ s but remained constant afterward. This was in contrast to the balloon test in Figure 7c, in which the increase of R continued. This can be explained due to the fact that the bladder was not voided due to the difficulty of positioning the device and sensor onto the bladder, thus the force imposed by the bladder onto the sensor was not reduced after $T = 40$ s.

The integration of force sensor with the device can compensate the loss of sensory signals in neurogenic UAB patients. The simplified diagram of the closed-loop control system in Figure 8c explains how the force sensor provides the sensory feedback signal to the patient for initiating the voiding. Future integration of force sensors with much softer substrate that can conform well to the vest seems necessary and will ease the application of the device onto the bladder.

3. Discussion

NiTi has been used as a safe implant material in several medical applications such as sutures, stents, guided wires, and valves.[5,47] The biocompatibility of NiTi was studied in several research works.[48,49] Furthermore, biocompatible silicone[50] can not only thermally isolate the NiTi SMA wires of the actuator from body organs but also can avoid any contact of body fluids with SMA wires. Future coating of the vest or replacing it with a biocompatible polymer[51] may be a solution to ensure the biocompatibility of the vest for future long term implantation of the device. Also 3D printing of anchor points with a biocompatible material,[52] and the use of biocompatible adhesives for fixation of anchor points on the vest,[53] can lead to a complete biocompatible actuator for future clinical applications. Possible usage of flexible biocompatible adhesives,[54] for fixing the vest to a wet surface like bladder, may be the possible option to avoid unwanted movement of the actuator and resulted friction between the vest and bladder surface.

SMA wires are capable of repeated deformations on the order of million cycles,[31] thus the actuator can endure for a long time after implantation. In order to show the repeatability of shape memory effect in the actuator, the contraction of the actuator by using antigravity experimental setup in Figure 3a is repeated for two times with and without the integrated force sensor. The plot of voiding percentage versus time is presented in Figure S4 (Supporting Information). A reduction of 5% (with force sensor) and 4.4% (without force sensor) was observed

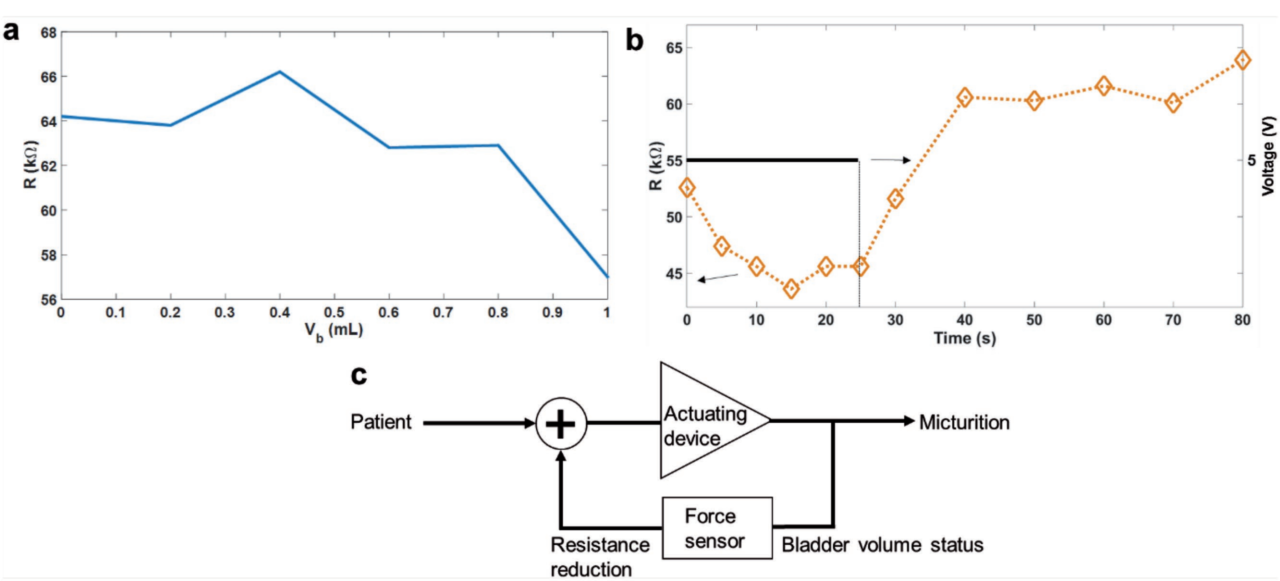

Figure 8. The in vivo test of the interlaced actuating device integrated with a force sensor in a rat. a) The effect of changes in the bladder volume on the resistance of the force sensor. b) The changes in resistance while 5 V actuation of the device. c) The schematic system for the actuating device integrated with a force sensor.

for the second actuation after 25 s of 5 V voltage application to SMA wires. A similar reduction at the voiding percentage was also observed previously for the parallel device.[14] Reduction of the applied voltage and the time duration of voltage application are suggested to reduce this effect.

Application of a ratchet/latching mechanism to compress the bladder might provide more force for the contraction, however, such devices require rigid substrates for the operation and are bulky.[55] Also usage of soft pneumatic actuators may suggest another approach for the contraction of bladder, but such devices need extra compressors for their operation.[56,57] The flexibility of our proposed actuator makes it suitable for the common keyhole surgeries on bladder, since it can be easily compressed to pass through the small incision and expanded inside the body for the implantation onto a bladder. The size of anchor points can be reduced further after coating of the vest with a biocompatible polymer to improve the strength of fingers of vest.

The interlaced device proposed in this study was able to void the bladder up to 23.59%. The residual urine in the bladder can lead to various complications.[58] For this reason, the conformability of the vest should be improved further in order to able to actuate the device multiple times continuously until a complete voiding is achieved. Therefore, using a thinner vest might improve the conformability of the vest. Lessening of the urethral resistance would also be advisable to avoid the backflow of urine toward kidneys due to the actuation of device; however, the gradual contraction by the device may not cause a serious issue in this regards.

4. Conclusion

This work presents a unique design for an SMA-based actuating device to physically contract the detrusor muscle and achieve a more than 20% voiding volume for the bladder. The proposed design of anchor points for fixing the SMA wires helps greatly in reducing the energy consumption of the device in comparison with the previously proposed design. Also, this method of anchorage for SMA wires permitted the free movement of SMA wires upon filling or voiding of the bladder, thus made it suitable for a wider range of bladder sizes in rats with similar body weight, and multiple actuation cycles. The design of SMA wires in an interlaced configuration improved the voiding percentage for about three times. The integration of the commercial sensor within the vest showed the possibility of providing a feedback control signal for neurogenic UAB patients with damaged nerves as well as detrusor muscle atrophy. This study can provide a proof-of-concept for the capability of this technology for future clinical applications.

5. Experimental Section

Force Sensor: FlexiForce A201 sensors were used to quantify the forces applied by the balloon or bladder while filling them with liquid, as well as, by SMA wires onto the vest. These commercial sensors have been used for several applications that require force sensing.[59,60] The force sensor has a thickness of 0.203 mm that consists of a layer of pressure-sensitive ink sandwiched between two layers of silver conductive materials.

Surgical Procedure: The experiments were performed on two adult female Sprague Dawley rats (First rat: 330 g, second rat: 294 g). The animal care and use procedures were approved by the Institutional Animal Care and Use Committee (IACUC) of the National University of Singapore. The methods were carried out in accordance with the R15-0592 protocol. The animal was anaesthetized by injecting ketamine-xylazine (75–10 mg kg^{-1}) into the intraperitoneal space. Carprofen (5 mg kg^{-1}) and normal saline (0.2–0.5 mL per 10 g) were injected subcutaneously to provide analgesic and prevent dehydration of the animal. Shaving of the abdominal/pelvic area was done prior to making an incision to access the urinary bladder and left ureter. Water recirculating heat pads were used to maintain the body temperature of the rat. A micro cannula was inserted into the left ureter for injecting normal saline to the urinary bladder for the experiments. The SMA-based device was positioned on the bladder wall and connected to the power source.

Density Measurement for the Liquid Voided from Rat's Bladder: The original contents in the bladder were completely emptied, and then the bladder was filled with normal saline. The bladder again was emptied and the voided liquid of 0.25 mL was collected in a micro tube. The micro tube containing the liquid was weighed by using a precision balance. After that, the micro tube was emptied completely and weighed. The 0.25 mL of the liquid had a weight of 0.2503 g.

Statistical Analysis: A total number of 2 rats were used for the experiments. The first rat was used for density measurement and testing of the actuating device for two times of actuation. The second rat was used for testing the integrated force sensor with the device. Three times of actuation was done for this device.

Supporting Information

Supporting Information is available from the Wiley Online Library or from the author.

Acknowledgements

The authors would like to acknowledge financial support from following research grants: NRF-CRP10-2012-01 "Peripheral Nerve Prostheses: A Paradigm Shift in Restoring Dexterous Limb Function" and NRF-CRP8-2011-01 "Self-powered body sensor for disease management and prevention-orientated healthcare" from the National Research Foundation (NRF), Singapore, and Faculty Research Committee (FRC) grant "Thermoelectric Power Generator (TEG) Based Self-Powered ECG Plaster—System Integration (Part 3)" at the National University of Singapore.
F.A.H. and C.L.: device design concept. F.A.H.: device modeling, fabrication, and characterization. F.A.H. and S.-C.Y.: experimental design and setup, and in vivo test data interpretation. G.G.L.G. and R.P.M.: animal surgeries. F.A.H.: in vivo test setup and device implantation on bladder. T.K.N., T.L.C.K., L.G.N., and P.L.: provided idea and motivation for bladder contraction device. N.V.T., S.-C.Y. and C.L.: principal investigators, study design, data interpretation.

Conflict of Interest

The authors declare no conflict of interest.

Keywords

anchorage and design, flexible electronics, force sensors, neurogenic under active bladder, shape memory alloy actuators

Received: July 12, 2017
Revised: September 15, 2017
Published online: November 15, 2017

[1] M. Zarinejad, Y. Liu, *Adv. Funct. Mater.* **2008**, *18*, 2789.
[2] L. An, W. M. Huang, *Mater. Sci. Eng., A* **2006**, *420*, 220.
[3] J. L. Pons, in *Emerging Actuator Technologies: A Micromechatronic Approach*, John Wiley & Sons, Ltd, Chichester, UK **2005**, Ch. 3.
[4] T. Yambe, S. Amae, S. Maruyama, Y. Luo, H. Takagi, S. Nanka, A. Tanaka, N. Kamiyama, R. Ohi, K. Tabayashi, H. Takeda, M. Yamada, S. Nitta, *J. Artif. Organs* **2001**, *4*, 88.
[5] L. Petrini, F. Migliavacca, *J. Metall.* **2011**, *2011*, 501483.
[6] S. Pittaccio, S. Viscuso, in *Smart Actuation and Sensing Systems—Recent Advances and Future Challenges* (Eds: G. Berselli, R. Vertechy, G. Vassura), InTech, Rijeka, Croatia **2012**, Ch. 4.
[7] K. Nishi, T. Kamiyama, M. Wada, S. Amae, T. Ishii, T. Takagi, Y. Luo, T. Okuyama, T. Yambe, Y. Hayashi, R. Ohi, *J. Pediatr. Surg.* **2004**, *39*, 69.
[8] J. M. Jani, M. Leary, A. Subic, M. A. Gibson, *Mater. Des.* **2014**, *56*, 1078.
[9] F. El Feninat, G. Laroche, M. Fiset, D. Mantovani, *Adv. Eng. Mater.* **2002**, *4*, 91.
[10] R. D. James, *Science* **2015**, *348*, 968.
[11] A. Nespoli, V. Dallolio, F. Stortiero, S. Besseghini, F. Passaretti, E. Villa, *Mater. Sci. Eng., C* **2014**, *37*, 171.
[12] T. Byun, T. S. Bae, K. H. Kim, *Adv. Sci. Technol. Lett.* **2016**, *141*, 19.
[13] S. Chonan, Z. W. Jiang, J. Tani, S. Orikasa, Y. Tanahashi, T. Takagi, M. Tanaka, J. Tanikawa, *Smart Mater. Struct.* **1997**, *6*, 410.
[14] F. A. Hassani, W. Y. X. Peh, G. G. L. Gammad, R. P. Mogan, T. K. Ng, T. L. C. Kuo, L. G. Ng, P. Luu, S.-C. Yen, C. Lee, *Adv. Sci.* **2017**, 1700143. https://doi.org/10.1002/advs.201700143.
[15] L. Xu, S. R. Gutbrod, A. P. Bonifas, Y. Su, M. S. Sulkin, N. Lu, H.-J. Chung, K.-In. Jang, Z. Liu, M. Ying, C. Lu, R. Chad Webb, J.-S. Kim, J. I. Laughner, H. Cheng, Y. Liu, A. Ameen, J.-W. Jeong, G.-T. Kim, Y. Huang, I. R. Efimov, J. A. Rogers, *Nat. Commun.* **2014**, *5*, 1.
[16] G. Cai, J. Wang, K. Qian, J. Chen, S. Li, P. S. Lee, *Adv. Sci.* **2017**, *4*, 1600190.
[17] S. Lee, Y. Inoue, D. Kim, A. Reuveny, K. Kuribara, T. Yokota, J. Reeder, M. Sekino, T. Sekitani, Y. Abe, T. Someya, *Nat. Commun.* **2014**, *5*, 1.
[18] S. Lee, A. Reuveny, J. Reeder, S. Lee, H. Jin, Q. Liu, T. Yokota, T. Sekitani, T. Isoyama, Y. Abe, Z. Suo, T. Someya, *Nat. Nanotechnol.* **2016**, *11*, 472.
[19] C. Pang, C. Lee, K.-Y. Suh. *J. Appl. Polym. Sci.* **2013**, *130*, 1429.
[20] Y. Liu, J. J. S. Norton, R. Qazi, Z. Zou, K. R. Ammann, H. Liu, L. Yan, P. L. Tran, K.-I. Jang, J. W. Lee, D. Zhang, K. A. Kilian, S. H. Jung, T. Bretl, J. Xiao, M. J. Slepian, Y. Huang, J.-W. Jeong, J. A. Rogers, *Sci. Adv.* **2016**, *2*, e1601185.
[21] X. Zhao, Q. Hua, R. Yu, Y. Zhang, C. Pan, *Adv. Electron. Mater.* **2015**, *1*, 1500142.
[22] X.-G. Yu, Y.-Q. Li, W.-B. Zhu, P. Huang, T.-T. Wang, N. Hu, S.-Y. Fu, *Nanoscale* **2017**, *9*, 6680.
[23] D. Kwon, T.-I. Lee, J. Shim, S. Ryu, M. S. Kim, S. Kim, T.-S. Kim, I. Park, *ACS Appl. Mater. Interfaces* **2016**, *8*, 16922.
[24] M. S. Sarwar, Y. Dobashi, C. Preston, J. K. M. Wyss, S. Mirabbasi, J. D. W. Madden, *Sci. Adv.* **2017**, *3*, e1602200.
[25] S. Gong, W. Schwalb, Y. Wang, Y. Chen, Y. Tang, J. Si, B. Shirinzadeh, W. Cheng, *Nat. Commun.* **2014**, *5*, 1.
[26] S. C. B. Mannsfeld, B. C.-K. Tee, R. M. Stoltenberg, C. V. H.-H. Chen, S. Barman, B. V. O. Muir, A. N. Sokolov, C. Reese, Z. Bao, *Nat. Mater.* **2010**, *9*, 859.
[27] C. J. Fowler, D. Griffiths, W. C. de Groat, *Nat. Rev. Neurosci.* **2008**, *9*, 453.
[28] K.-E. Andersson, A. Arner, *Physiol. Rev.* **2004**, *84*, 935.
[29] W. C. de Groat, C. Tai, *Bioelectron. Med.* **2015**, *2*, 25.
[30] M. B. Chancellor, in *The Underactive Bladder* (Eds: M. B. Chancellor, A. C. Diokno), Springer International Publishing, Switzerland **2016**, Ch. 6 and 9.
[31] DYNALLOY, Inc., *Technical Characteristics of FLEXINOL Actuator Wires*, http://www.dynalloy.com/pdfs/TCF1140.pdf (accessed: September 2017).
[32] Object, FullCure Materials, http://svl.wpi.edu/wp-content/uploads/2014/04/FullCure_Letter_low-1.pdf (accessed: September 2017).
[33] Stratasys, PolyJet Materials Data Sheet, http://usglobalimages.stratasys.com/Main/Files/Material_Spec_Sheets/MSS_PJ_PJMaterialsDataSheet.pdf?v=635785205440671440 (accessed: September 2017).
[34] Shin-Etsu Silicone Inc., *Characteristic Properties of Silicone Rubber Compounds*, www.shinetsusilicone-global.com/catalog/pdf/rubber_e.pdf (accessed: September 2017).
[35] J. J. Licari, in *Coating Materials for Electronic Application: Polymers, Processes, Reliability, Testing*, Noyes Publications/William Andrew, Inc., Norwich, NY **2003**, Ch. 1.
[36] E. Briese, *Neurosci. Biobehav. Rev.* **1998**, *22*, 427.
[37] H. N. Bhargaw, M. Ahmed, P. Sinha, *Trans. Nonferrous Met. Soc. China* **2013**, *23*, 2329.
[38] C. Li, G. Guan, F. Zhang, S. Song, R. K. Wang, Z. Huang, G. Nabi, *Biomed. Opt. Express* **2014**, *5*, 4313.
[39] E. Briese, *Neurosci. Biobehav. Rev.* **1998**, *22*, 427.
[40] G. M. Herrera, A. L. Meredith, *PLoS One* **2010**, *5*, e12298.
[41] S. Lee, H. Wang, Q. Shi, L. Dhakar, J. Wang, N. V. Thakor, S.-C. Yen, C. Lee, *Nano Energy* **2017**, *33*, 1.
[42] Q. Shi, T. Wang, C. Lee, *Sci. Rep.* **2016**, *6*, 1.
[43] R. D. Walters, G. McMurray, A. F. Brading, *Neurourol. Urodyn.* **2006**, *25*, 62.
[44] S. J. A. Majerus, P. C. Fletter, M. S. Damaser, S. L. Garverick, *IEEE Trans. Biomed. Eng.* **2011**, *58*, 763.
[45] S. J. A Majerus, P. C. Fletter, E. K. Ferry, H. Zhu, K. J. Gustafson, M. S. Damaser, *PLoS One* **2017**, *12*, e0168375.
[46] Tekscan, FlexiForce Standard Model A201, https://www.tekscan.com/product-group/embedded-sensing/force-sensors (accessed: September 2017).
[47] T. Duerig, A. Pelton, D. Stockel, *Mater. Sci. Eng., A* **1999**, *273–275*, 149.
[48] S. Shabalovskaya, J. V. Humbeeck, in *Shape Memory Alloys for Biomedical Applications* (Eds: T. Yoneyama, S. Miyazaki), Woodhead Publishing Limited, Cambridge **2009**, Ch. 9.
[49] S. Kujala, A. Pajala, M. Kallioinen, A. Pramila, J. Tuukkanen, J. Ryhanen, *Biomaterials* **2004**, *25*, 353.
[50] D. Fallahi, H. Mirzadeh, M. T. Khorasani, *J. Appl. Polym. Sci.* **2003**, *88*, 2522.
[51] F. Yao, W. J. Kao, *Expert Opin. Drug Delivery* **2010**, *7*, 429.
[52] Stratasys, PolyJet Materials/System Matrix, http://global72.stratasys.com/~/media/Main/Files/Material_Spec_Sheets/MSS_PJ_System_Matrix.ashx#_ga=2.190735531.122203221.1505019955-928720846.1505019955 (accessed: September 2017).
[53] S. M. Tavakoli, D. A. Pullen, S. B. Dunkerton, *Assembly Autom.* **2005**, *25*, 100.
[54] J. Li, A. D. Celiz, J. Yang, Q. Yang, I. Wamala, W. Whyte, B. R. Seo, N. V. Vasilyev, J. J. Vlassak, Z. Suo, D. J. Mooney, *Science* **2017**, *357*, 378.
[55] B. Utter, J. Luntz, D. Brei, D. Teitelbaum, M. Okawada, E. Miyasaka, *Proc. SPIE* **2009**, *7288*, 72881A.
[56] R. V. Martinez, A. C. Glavan, C. Keplinger, A. I. Oyetibo, G. M. Whitesides, *Adv. Funct. Mater.* **2014**, *24*, 3003.
[57] E. T. Roche, M. A. Horvath, I. Wamala, A. Alazmani, S.-E. Song, W. Whyte, Z. Machaidze, C. J. Payne, J. C. Weaver, G. Fishbein, J. Kuebler, N. V. Vasilyev, D. J. Mooney, F. A. Pigula, C. J. Walsh1, *Sci. Transl. Med.* **2017**, *9*, eaaf3925.
[58] M. May, S. Brookman-Amissah, B. Hoschke, C. Gilfrich, K.-P. Braun, F. Kendel, *J. Urol.* **2009**, *181*, 2540.
[59] M. Monga, J. Premoli, N. Skemp, W. Durfee, *J. Endourol.* **2004**, *18*, 654.
[60] A. Nag, S. C. Mukhopadhyay, J. Kosel, *Sens. Actuators, A* **2016**, *251*, 148.

